REPEATED FLARING FROM LOOP-LOOP INTERACTION

S. POHJOLAINEN
Tuorla Observatory, Väisälä Institute for Space Physics and Astronomy, University of Turku, Väisäläntie 20, FIN-21500 Piikkiö, Finland; spo@astro.utu.fi

(Solar Physics - accepted Nov. 2002)

Abstract. A series of solar flares was observed near the same location in NOAA active region 8996 on May 18–20, 2000. A detailed analysis of one of these flares is presented where the emitting structures in soft and hard X-rays, EUV, Hα, and radio at centimeter wavelengths are compared. Hard X-rays and radio emission were observed at two separate loop footpoints, while soft X-rays and EUV emission were observed mainly above the nearby positive polarity region. The flare was confined although the observed type III bursts at the time of the flare maximum indicate that some field lines were open to the corona. No flux emergence was evident but moving magnetic features were observed around the sunspot region and within the positive polarity (plage) region. We suggest that the flaring was due to loop-loop interactions over the positive polarity region, where accelerated electrons gained access to the two separate loop systems. The repeated radio flaring at the footpoint of one loop was visible because of the strong magnetic fields near the large sunspot region while at the footpoint of the other loop the electrons could precipitate and emit in hard X-rays. The simultaneous emission and fluctuations in radio and X-rays – in two different loop ends – further support the idea of a single acceleration site at the loop intersection.

1. Introduction

Homologous flares are usually defined as members of a series that have the same main footpoints (same location) and that show similar (impulsive) time evolution in radio emission at centimeter and millimeter wavelengths. As radio emission at these wavelengths is mostly due to accelerated energetic particles gyrating along the magnetic field lines, a good correlation with hard X-rays (same particle population) is normally found. The presence of a large sunspot seems to be a necessary condition for homologous flaring, and the time interval between flares has been observed to vary from hours to a few days, see examples and summaries in e.g. Martres (1989), Gaizauskas (1986), and Cliver and Wefer (1981).

The main question concerning repeated flaring is whether it is due to continual shearing and reconnection of similar structures – where maybe not all of the magnetic free energy is released – or if it is due to repeatedly emerging flux. The emerging flux scenario in which

Table I. Summary of flares in AR 8996 during May 18–20, 2000

Flare	Time of maximum at 17 GHz	Max. flux 17 GHz	BATSE peak c/s/2000 cm^2	GOES class	Type III emission
A	May 18, 2000 22:59:35	150 sfu	42417	C6.0	22:59–23:00
B	May 18, 2000 23:48:56	15 sfu	1466	C5.3	
C	May 18, 2000 23:52:34	15 sfu	710	C5.0	
D	May 19, 2000 00:39:16	25 sfu	2839	C8.0	
E	May 20, 2000 01:06:27	80 sfu	19663	C7.5	01:06–01:07

the preflare conditions are reformed after each flare has gained more support recently (Ranns et al., 2000; Zhang and Wang, 2002; Sterling and Moore, 2001; Howard and Svestka, 1981), although simulations of continuous shear-increasing footpoint motions (Choe and Cheng, 2000) and analyses on the changes in the flare homology in connection with magnetic shear (Machado, 1985) have been presented as well.

A series of solar flares were observed to occur in the same location within a complex magnetic topology of AR 8996 during May 18–20, 2000. The same location (S21W11 on May 18, S20W25 on May 20), similar radio spectra, and temporal evolution in radio and in X-rays suggest that the repeated flaring could be called homologous. Due to the sparsity of data on all of the five flares we will first give an overview on all events in the series, and then concentrate in the analysis of one of the flares that had sufficient imaging data available. A possible scenario for the flaring is then presented, based on the observations.

2. Instrumentation

The analysis was done using EUV images from the EIT telescope (Delaboudinière et al., 1995) on board the *Solar and Heliospheric Observatory (SOHO)*, solar magnetograms from the *SOHO* MDI instrument (Scherrer et al., 1995), soft X-ray images from the *Yohkoh* SXT (Tsuneta et al., 1991), hard X-ray imaging from the *Yohkoh* HXT (Kosugi et al., 1991), Hα images provided by the Space Environment Center (SEC) at NOAA, and 17 and 34 GHz radio imaging data from the Nobeyama Radioheliograph (NoRH) (Nakajima et al., 1994).

Full disk radio flux density at 1, 2, 3.75, 9.4, 17, and 35 GHz were provided by the Nobeyama polarimeters (NoRP) (Nakajima et al., 1985). The Hiraiso Radio Spectrograph (HiRAS) in Japan records the radio flux at 25–2500 MHz. The *Geostationary Operational Environ-*

mental Satellites (GOES) recorded the full Sun soft X-ray flux, and the BATSE detector on board the *Compton Gamma Ray Observatory* (Fishman et al., 1994) observed the flares in hard X-rays.

The radio flare locations were determined from the Nobeyama Radioheliograph 17 GHz images. The spatial resolution at this frequency is 10 arcsec and the temporal resolution 1 s. The *Yohkoh* SXT and *SOHO* EIT resolutions vary from 2.5 arcsec to 10 arcsec, depending on the observing mode.

3. Flares A–E

The flares were first discovered in the daily flux curves of the Nobeyama Radioheliograph (NoRH) on May 18–20, 2000, see Figure 1. We picked flares originating from the same location and that exceeded the 0.01 unit correlation level, which indicates relatively large radio fluxes in cm- and mm-waves. We thus ended up with five flares (A–E). The *GOES* flux curves show that the soft X-ray flux level remained relatively low during all of the five radio flares, between C5.0 and C8.0. The NGDC reports type III radio emission during flares A and E. The NOAA SEC Hα images show that the main sunspot region was surrounded by a large number of dark filaments on May 18 but by May 20 many of them had disappeared. The positive polarity field ahead of the sunspot remained a bright plage region all this time. The flare characteristics are summarized in Table I.

EIT images are available at regular time intervals, and the images show a complex active region with several loop systems that did not change much during the two days (Figure 2). The radio flare positions are superposed on the EIT 195 Å images in white contours. The radio emission sites seem to be located at one footpoint of the most prominent EUV loop (indicated with small arrows in Figure 2A), but in the analysis we found no evidence of any activity along this loop or near the other footpoint of this loop. The filaments seen in the Hα images are also visible as dark lanes in some of the EUV images. The location of the radio flares was on the west (leading negative polarity) side of a large sunspot region ahead of which was a narrow positive polarity region (see magnetograms in Figure 2). The field strengths at photospheric level – as we cannot measure it at the heights of the radio emission – near the sunspot were ~ -2300 G at maximum and 200–500 G in the positive polarity field.

Flares A and D occurred during *Yohkoh* satellite night time and most of the time during flares B and C *Yohkoh* was pointed at another region. This leaves only flare E well covered in X-ray images. However,

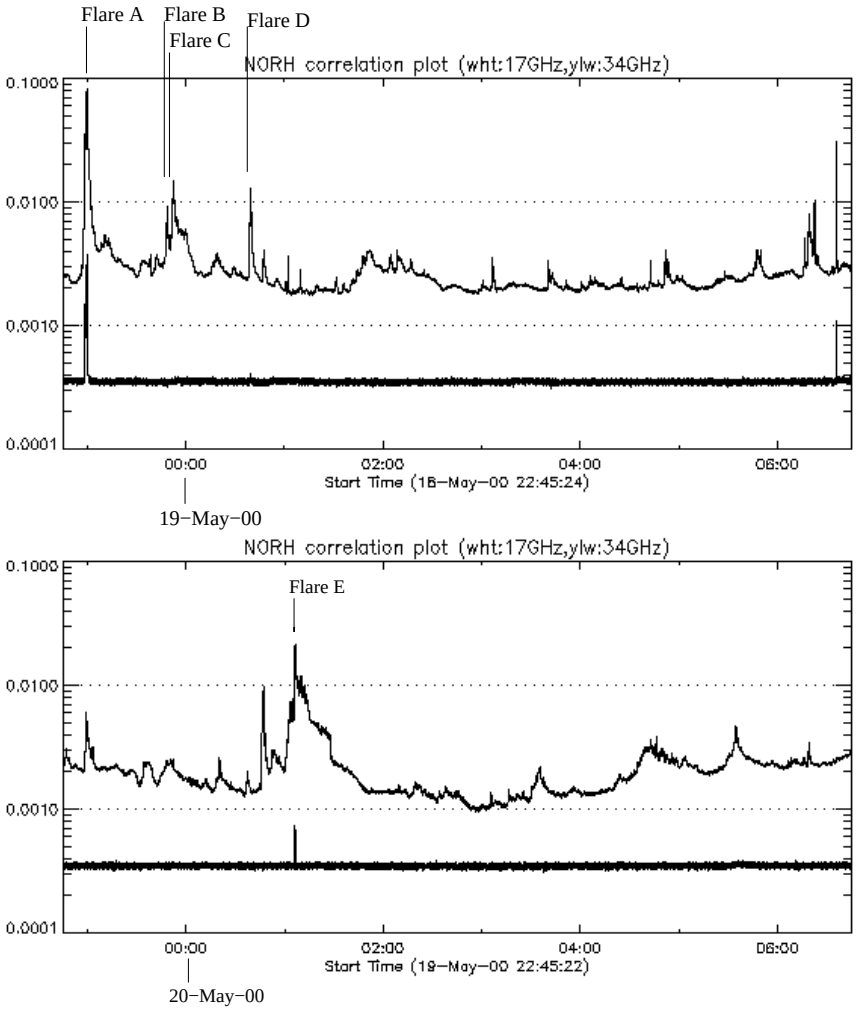

Figure 1. Nobeyama 17 and 34 GHz correlation plots (upper and lower curves, respectively) for the two observing days on 2000 May 18, 22:45 UT – 2000 May 19, 06:50 UT and 2000 May 19, 22:45 UT – 2000 May 20, 06:50 UT. The times of flares A, B, C, D and E are marked on the plots. These were strong radio flares that exceed the 0.01 correlation level at the radioheliograph. (The flare on 2000 May 19 at 06:35 UT was not located in the same region as the other flares.)

the SXT images between May 18 and May 20 reveal several loops and loop systems that get bright at separate time intervals but have their footpoints in the same locations. Some of these are shown in Figure 3.

The temporal evolution of the radio flux densities and BATSE hard X-ray counts were similar. The radio and hard X-ray flares had 1–2 minute durations and they showed fluctuations with timescales from 3 to 22 seconds between the flux/count rate peaks. The spectral turn-over

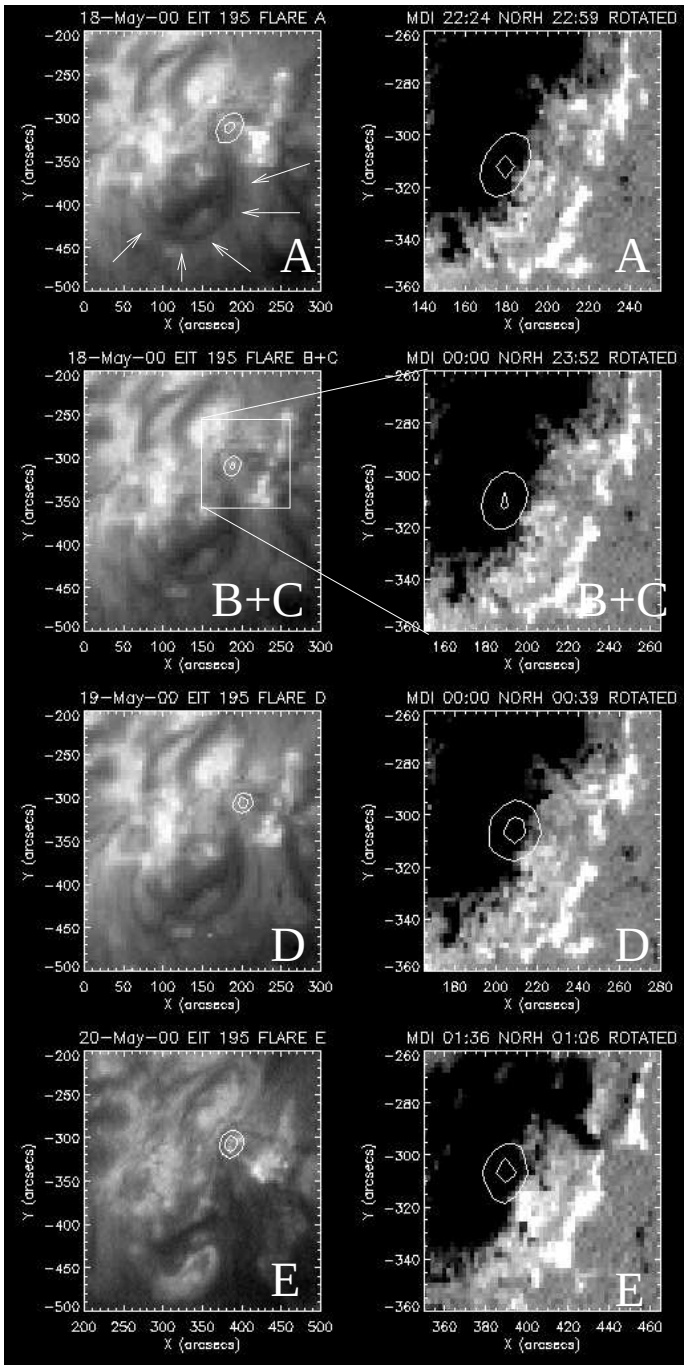

Figure 2. Radio flare locations for flares A-E: On the left are the NoRH 17 GHz radio burst locations (white contours) plotted over the neareast EIT 195 Å images. On the right are the same (rotated, see Howard, Harvey, and Forgach, 1990) radio burst locations plotted over the nearest MDI magnetograms (only field strengths from -200 G to 200 G are shown). The EIT 195 Å images all show a 300×300 arcsec field of view with rotation effects taken into account and the magnetograms are 115×100 arcsec submaps of the same region with rotated radio flare locations. The large EUV loop mentioned in the text is indicated with small arrows in the flare A image.

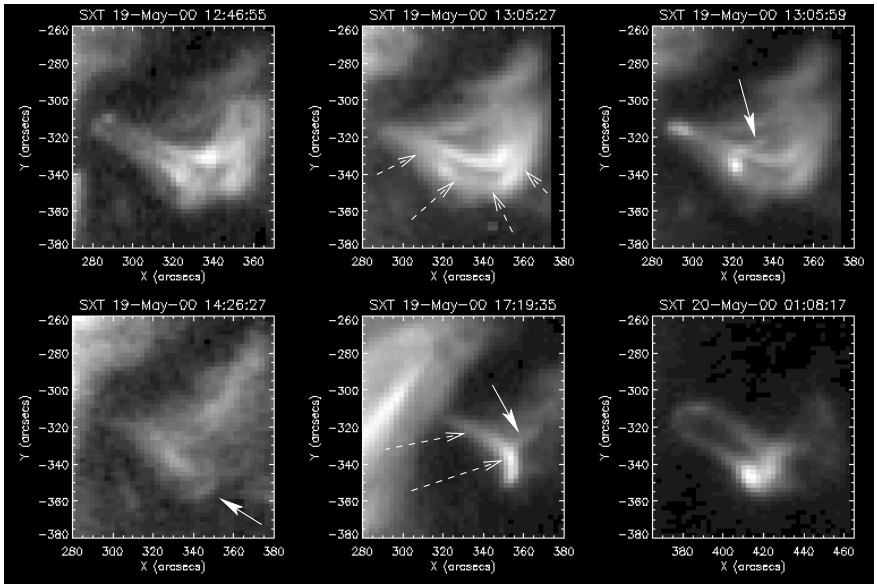

Figure 3. *Yohkoh* SXT images of the flaring region during May 19 – May 20, 2000. Several loops and loop systems connecting the sunspot region (negative polarity) and the plage region (positive polarity) are visible in the images throughout the days, as they brighten at separate time intervals. Two of the long connecting loops are indicated by white dashed-line arrows. Some smaller loops, almost perpendicular to the long connecting loops, are indicated by white solid-line arrows.

frequency at radio wavelengths for all the flares was between 9.4 and 17 GHz (determined from the NoRH and NoRP observations). The radio images did not show any shift in the emission locations (within the 10 arcsec spatial resolution). The NoRH flux densities and the *CGRO* BATSE hard X-ray count rates for flares A–D are presented in Figure 4, and for flare E in Figure 8.

4. Flare E on May 20, 2000

4.1. Radio – soft X-rays

The GOES full disk soft X-ray flux curve for flare E on May 20, 2000 is presented in Figure 5. Unfortunately the first flux changes occurred during *Yohkoh* night time. Flare E was first seen in radio and hard X-rays at 01:06:00 UT, but the soft X-ray images show that the nearby positive polarity region had already brightened well before that (area with saturated pixels in Figure 6c, due to long exposure time). Also in the last images before *Yohkoh* night time at 00:18 UT (Figures 6a and b) some overlying loop structures are visible. The positive polarity

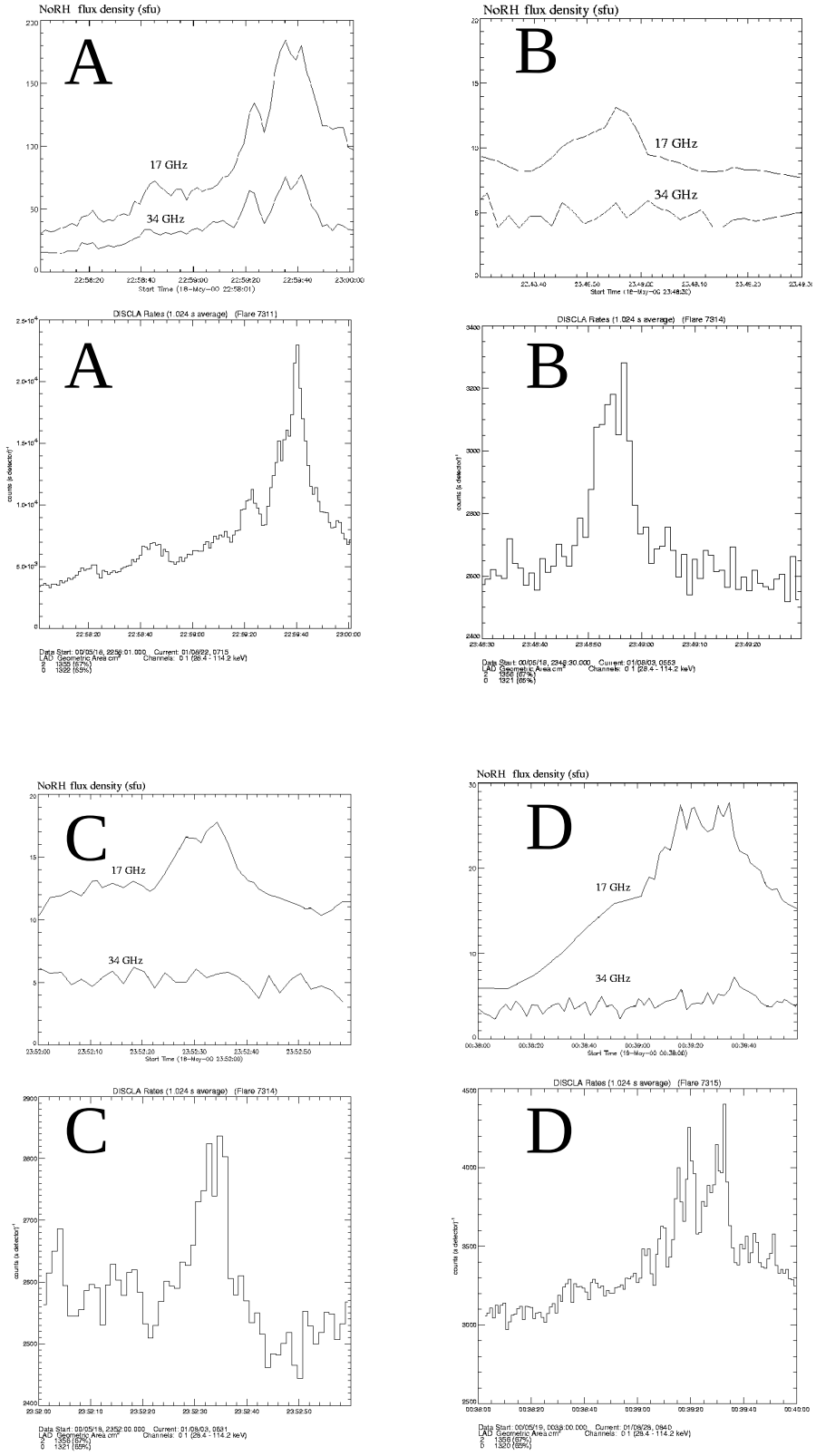

Figure 4. Radio and hard X-ray flux curves for flares A, B, C, and D. The flux curves for flare E are presented in Figure 7. The bursts have similar short 1-2 minute durations, show fluctuations in the rising phase, and the radio and hard X-ray emission peaks show good temporal correlation.

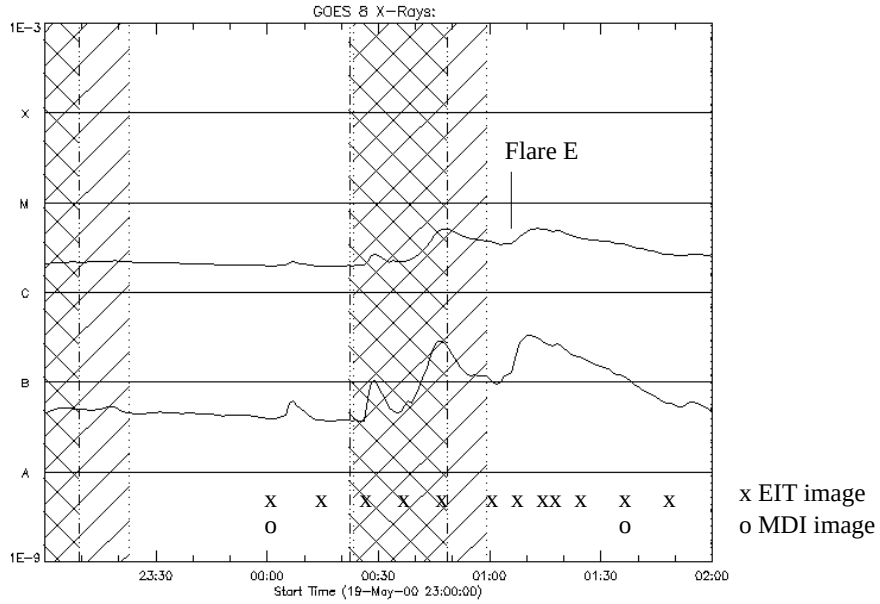

Figure 5. Summary of observations for flare E: GOES soft X-ray flux curves for 19 May, 2000 23:00 UT – 20 May, 2000 02:00 UT, with the times of the *SOHO* EIT ('x') and MDI images ('o'). The *Yohkoh* satellite night times (hatched areas) and the South Atlantic Anomaly intervals (dashed hatched areas) represent times when no *Yohkoh* observations are available.

region was connected to the radio flare location by at least two distinct loop structures: In the SXT images the radio flare site (indicated by a black arrow in Figure 6c) is in one end and the brightened positive polarity region in the other. About 10 minutes after the radio flare an extended bright region was visible in connection with the upper loop (Figures 6e and f).

Figure 7 shows the SXT lightcurves taken with the AlMg filter for the five different regions marked in Figure 6d (Boxes 1–5). From these it is evident that region 1 brightens at the time of the radio flare and then slowly decays, while practically all the other regions continue to brighten. Region 2 was already very bright when the radio flare occurred, indicating possible earlier flaring in the positive polarity plage region (in accordance with the GOES time plot). Similar flux curves for the NoRH 17 GHz radio emission inside the same regions were also calculated. Most of the radio flare flux originated from Box 1 (45 sfu increase in the region), although region 2 got brighter as well (0.4 sfu increase). The locations of the loops (regions 3 and 4) showed flux fluctuations similar to the main flare site in region 1, but their intensity was in the scale of 0.1 sfu which was very near the noise level.

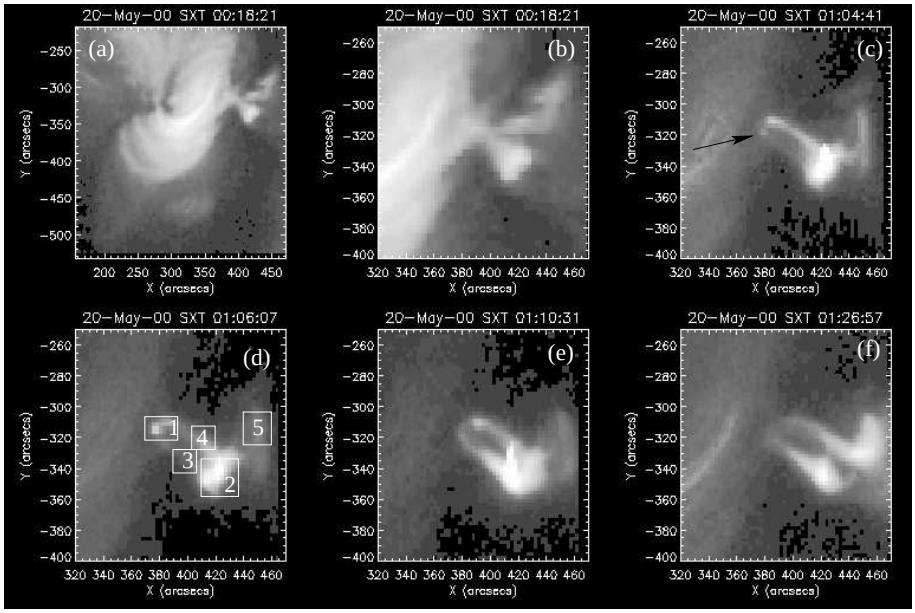

Figure 6. *Yohkoh* SXT images of the flaring region: (a) shows a large field of view of the region at 00:18:21 UT just before *Yohkoh* entered satellite night time and the GOES flux started to rise, (b) is an enlargement of the previous 00:18:21 UT image, (c) is the first SXT image after satellite night time ended at 01:04:41 UT, with black arrow pointing to the radio flare location (d) the SXT image during the rising phase of the flare, at 01:06:07 UT shows the small loop-like structure that began to form inside Box 1, the bright plage area (Box 2), and the lower (Box 3) and upper (Box 4) connecting loops between these two regions, (e) and (f) showing the later development of the flaring region at 01:10:31 UT and 01:26:57 UT, respectively.

4.2. Radio – hard X-rays

The 17 and 34 GHz radio flux started to rise around 01:06:04 UT and the impulsive phase lasted for less than one minute. The radio spectrum had a turn-over frequency between 9.4 and 17 GHz, as in the other flares in the series. The 17 GHz radio flux density from the flare region and the BATSE hard X-rays had similar temporal evolution, with periodic 3–4 s fluctuations, see Figure 8. In addition, the NoRP 2 GHz observations showed decimetric pulsations. The HiRAS spectral observations recorded type III radio bursts at 50—1000 MHz around 01:06–01:07 UT. These were also visible with the NoRP single frequency observations at 1 GHz.

Flare E was the only event with high enough count rates in the lowest *Yohkoh* HXT energy channel (14-23 keV) to allow construction of images of the emitting region. The HXT images at the times of count rate peaks show that the hard X-ray emission sites were shifted between

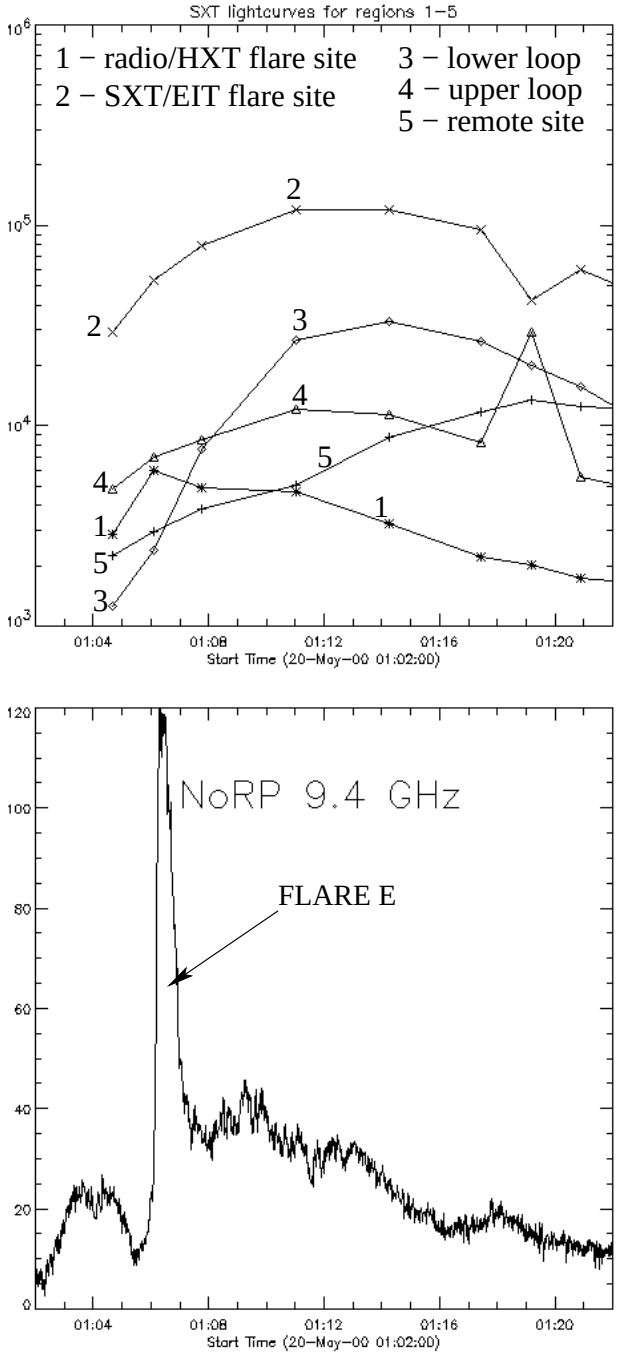

Figure 7. Top: *Yohkoh* SXT AlMg filter light curves (DN/s) calculated for the different SXT regions (Boxes 1-5) shown in Figure 6. The radio flare E was located in Box 1 at 01:06–01:07 UT for which time period only one SXT AlMg image is available. Bottom: NoRP 9.4 GHz flux density curve (sfu) showing radio flare E.

the peaks. The HXT peaks at 01:06:13 and 01:06:23 UT appear to be located further along the upper loop than at 01:06:11 and 01:06:19 UT, respectively, see Figure 8.

Figure 9 (top image) shows the active region in soft X-rays, together with the hard X-ray and radio source positions. The hard X-ray (HXT) emission source is located near the upper loop footpoint and the radio emission source is located east of it. In the soft X-ray images as well as in the EIT 284 Å image at 01:06:00 UT there is at least one less bright pixel visible in between the upper and lower loops – this 'gap' is even more evident in the EIT 304 Å image at 01:18 UT after the flare. We suggest that the radio and hard X-ray emission sites are not the opposite ends of a tiny loop but instead they are two separate footpoints of the longer loops that connect to the nearby positive polarity plage region – the footpoints simply lie so near to each other that they are almost unresolved. This interpretation has also effects for the observed HXT emission displacements: if the tiny loop-like structure is in reality two separate footpoints of the same polarity, hard X-rays from 'higher along the tiny loop' should be 'deeper down from the footpoint area'. It is most unfortunate that we do not have any TRACE images of this region that might resolve the footpoint area better.

4.3. Magnetic connectivity and evolution

When looking at the soft X-ray loop structures superposed on the *SOHO* MDI magnetograms the loop connections become more evident, see Figure 9 (bottom four images). In the first image the SXT contours show the loops at the start of the flare and the arrows point to the regions that brighten in the impulsive phase. The arrow pointing to the negative polarity field is the location of the radio emission site. In the next image (during the radio/hard X-ray flare) the lower SXT loop has also brightened. In the third image (right after the impulsive flare phase) the two-loop structure is even more evident. In the last (post-flare 'tail') image the upper loop expands towards the north. This evolution is also visible in Figure 6f.

The two connecting loops that were shown in Figure 3 (white dashed-line arrows) intersect above the lower part of the positive polarity field. The positive polarity footpoint of the upper loop is very near the intersection region and due to the enhanced loop top emission the positive polarity footpoint emission is not well resolved. The magnetograms confirm that the other set of footpoints (i.e., the radio-emitting and the hard X-ray emitting) lie on the negative polarity field. The field strengths however differ: the radio emitting footpoint is approximately at -900 – -1300 G and the hard X-ray emitting footpoint at -100 –

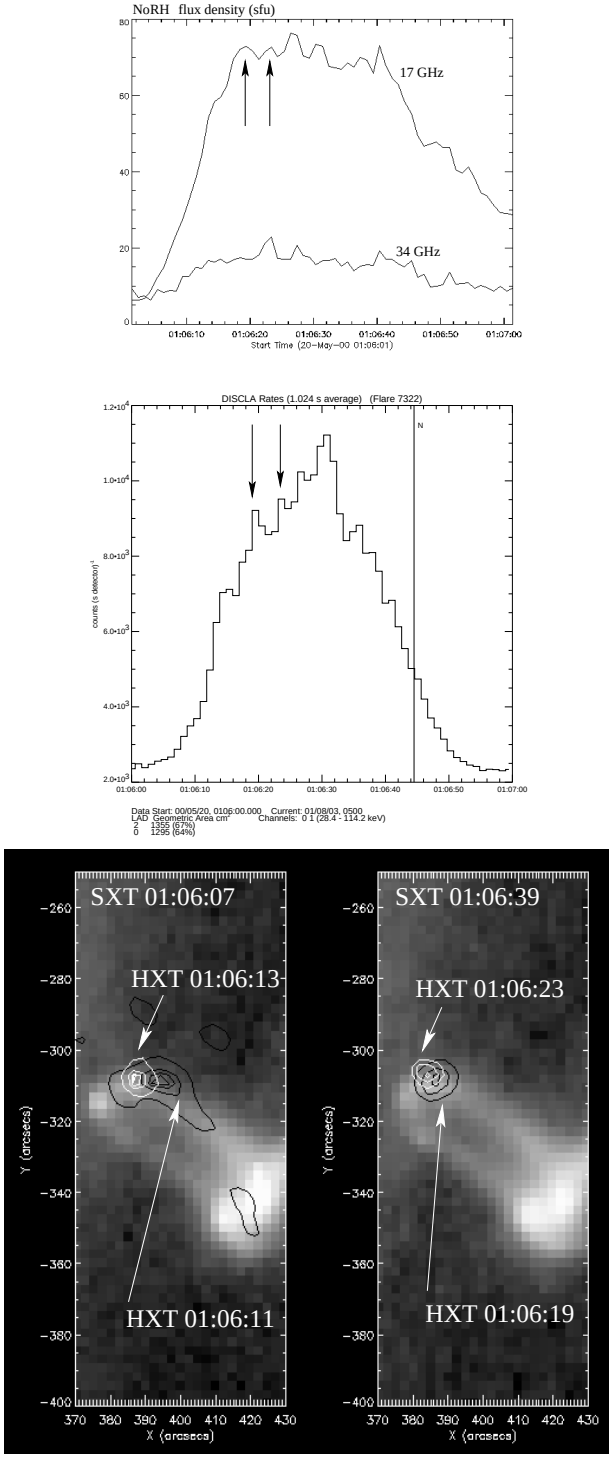

Figure 8. On top: Nobeyama radio flux at 17 and 34 GHz from the flare site (a 50×60 arcsec box around the flare region) and BATSE 28–114 keV counts during flare E. Fluctuations are seen in the radio flux, corresponding to step-like increases in hard X-rays. Bottom: Hard X-ray source positions at four different times during the flare, superposed on the soft X-ray images. The *Yohkoh* HXT source positions are shifted between the count rate peaks, but all sources are located near the end of the upper loop. The hard X-ray burst locations at 01:06:19 and 01:06:23 UT (times indicated by arrows in the radio and hard X-ray curves) are shown in the bottom right image).

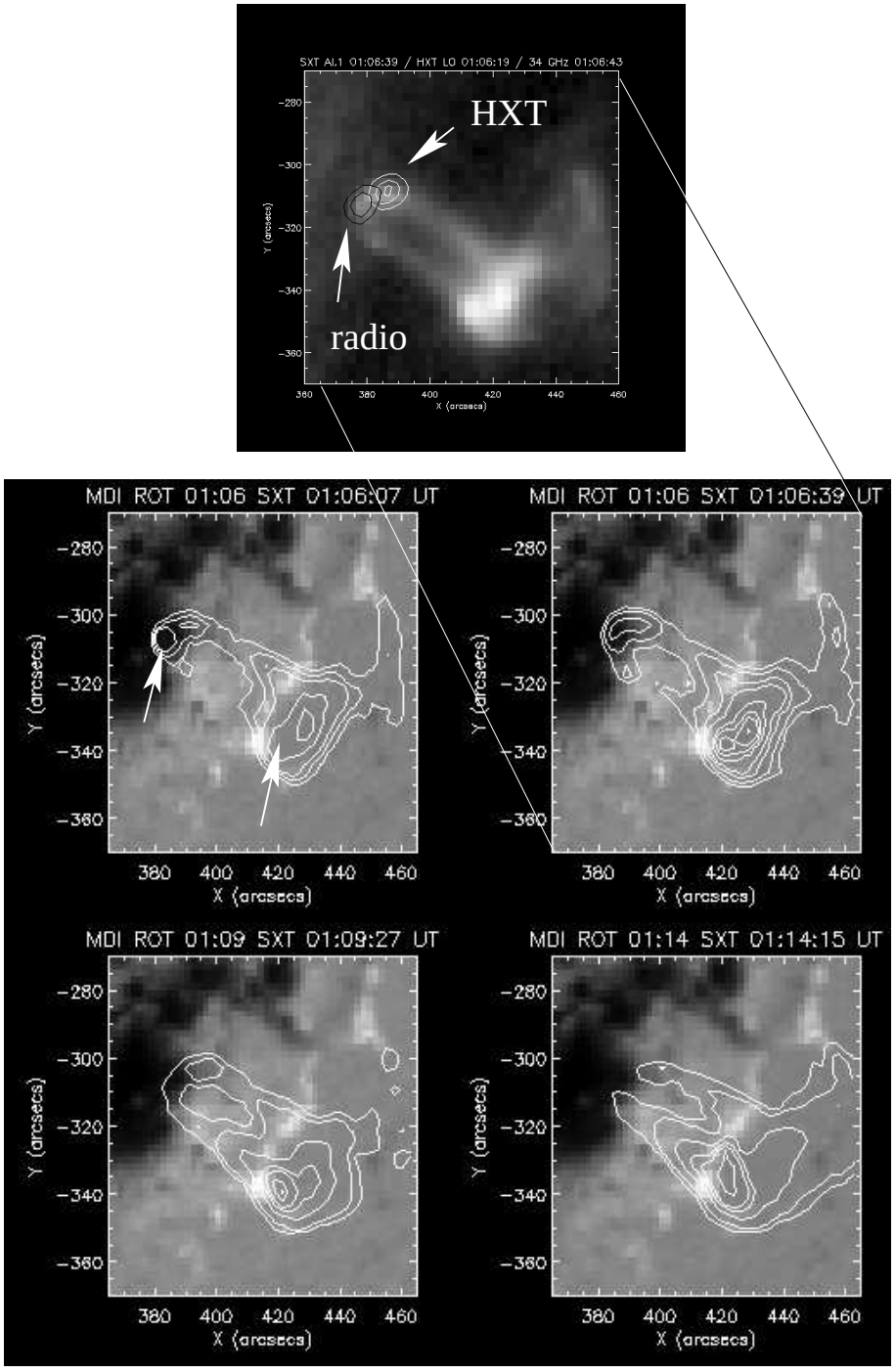

Figure 9. On top: Hard X-ray source location (white contours) and radio flare location (black contours) superposed on the SXT image from the time of the radio/hard X-ray flare. Bottom: SXT structures (white contours) superposed on MDI magnetograms at four different times: 01:06:07 UT (beginning of flare), 01:06:39 UT (during flare), 01:09:27 UT (3 minutes after impulsive phase), 01:14:15 UT (post-flare 'tail'). The arrows in the first image at the beginning of the flare point to the regions that brighten in the impulsive phase.

−350 G. The magnetic field strength in the nearby positive polarity region ranges between 230 and 590 G.

The *SOHO* MDI magnetograms in Figure 10 were taken at 00:00 UT and 01:36 UT on May 20, well before and after the flare. The large time gaps (the full disk magnetograms are taken every 96 minutes) and the fact that many of the magnetic features are weak (MDI 1-σ noise level is about 20 G) make the analysis difficult, but mainly two things are evident from the magnetograms taken on May 19–20: First, there is a flow of magnetic flux from the sunspot region towards the positive polarity field. The directions of the flows are indicated by black arrows in Figure 10. The flows include small traces of emerging positive polarity flux in between the sunspot and the plage region. Second, there are positional shifts in the locations of the magnetic flux elements inside the positive polarity field. The two positive polarity areas indicated by white arrows in Figure 10 become more separated in time, and it also looks like some of the positive polarity flux elements merge with each other.

A quantitative analysis of the magnetograms verifies that the pre-flare and post-flare magnetic field near the positive polarity loop footpoint region does not change much and both before and after the flare the box area A1 (Figure 10) contains only positive magnetic flux. Inside box A2, which is the lower part of the plage area and contains some loop footpoints, there are both positive and negative flux elements but no significant flux changes are observed. The other box areas B1 and B2 show the development in the upper part of the positive polarity region and the region in between the positive polarity and the negative polarity sunspot region, respectively. Box B1 contains mainly positive polarity elements, and the three pixels that contain low strength negative polarity elements are all located west of the plage region. The B2 area is part of the magnetic flux flow and emerging flux region around the sunspot and also contains only positive flux elements. The large increase in the B2 magnetic field strength is caused by the flux flows that reach the left side of the box area. One should note that small flux changes and emerging flux could be diluted by the MDI resolution and also that the large time difference between the flare and the next MDI image could give the field time to rearrange itself. The total unsigned magnetic fluxes before and after the flare in each box are given in Table II.

The field strength near the footpoint area at the negative polarity sunspot region remained high, although the field strength diminished in some pixels (region within the white circle in Figure 10) in the magnetogram before the flare. The drop was from -920 G to -740 G, and the field strength was again -990 G after the flare.

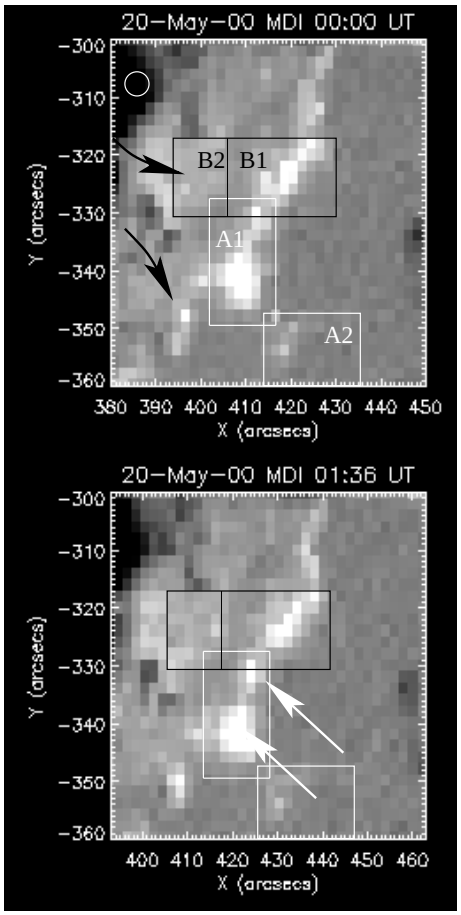

Figure 10. SOHO MDI magnetograms on 20 May 2000 at 00:00 UT (one hour before the flare) and at 01:36 UT (half an hour after the flare). Black arrows show the direction of the magnetic flux flow and white arrows point to the regions where the magnetic flux elements showed movement (positional shift). The boxed regions show the areas for which the magnetic field was analysed in detail (see text).

Table II. Pre-flare and post-flare magnetic field on May 20, 2000. The MDI pixel size is 1.98 arcsec × 1.98 arcsec and the noise level about 20 G.

	Pre-flare total flux (Mx)	Post-flare total flux (Mx)	Field strength increase in region (Gauss)
Region A1 (77 pixels)	2.17×10^{22}	2.21×10^{22}	280
Region A2 (77 pixels)	0.42×10^{22}	0.43×10^{22}	55
Region B1 (77 pixels)	1.79×10^{22}	1.82×10^{22}	180
Region B2 (42 pixels)	0.52×10^{22}	0.60×10^{22}	980

In order to track the magnetic field evolution around the positive polarity region and to get an idea on the scale of the moving magnetic features a small area was selected, indicated by the boxes in Figure 11, and the total magnetic field strength inside the box was calculated during 40 hours starting from May 18, 2000 19:12 UT. The total field strength and the maximum field strength values show that some 10 hours before flare E the field inside the box area started to get stronger and also started to show higher maximum values. This was mainly due to flux concentration (single pixels started to show higher values) and moving magnetic features entering the box from below. The total field change before flare E was from 8000 G to 9200 G.

In summary the positive polarity plage region seems to be getting stronger and gaining magnetic flux while it also undergoes spatial changes. The negative polarity sunspot region is losing some of the restored magnetic energy and the area in between the plage and the sunspot is in constant motion, with emerging and moving positive polarity flux elements.

5. Summary and discussion

The sequence of flares that occurred in the same location within the two days were remarkably similar in temporal evolution and in spectral characteristics. One of the flares was analysed in detail. The flare occurred in the vicinity of a large sunspot region, and the radio and hard X-ray emissions seemed to originate from two different footpoint locations, but both in the negative polarity field region. The footpoint separation was less than 20 arcsec (two times the radio resolution). The SXT and EIT images from May 18–20 showed two long-living loops with positive polarity footpoints in the nearby plage region. These loops seemed to intersect above the lower parts of the positive polarity field. Some smaller, almost vertical loops were visible in some of the earlier images but these did not connect to the sunspot region (as shown in Figure 3).

The analysis of the magnetograms before and after the flare showed that there was no evident flux emergence inside the positive polarity region. The flux emergence and flows around the sunspot region seemed to end as they approached the positive polarity (plage) region – Zirin (1983) has shown previously that plages as a whole do not move. Spatial movement of the flux elements and strengthening of the positive polarity field *within* the plage region were observed in our case.

No ejected material was visible in the images during the flare. This could be due to the poor image cadence in EUV and soft X-rays, but the

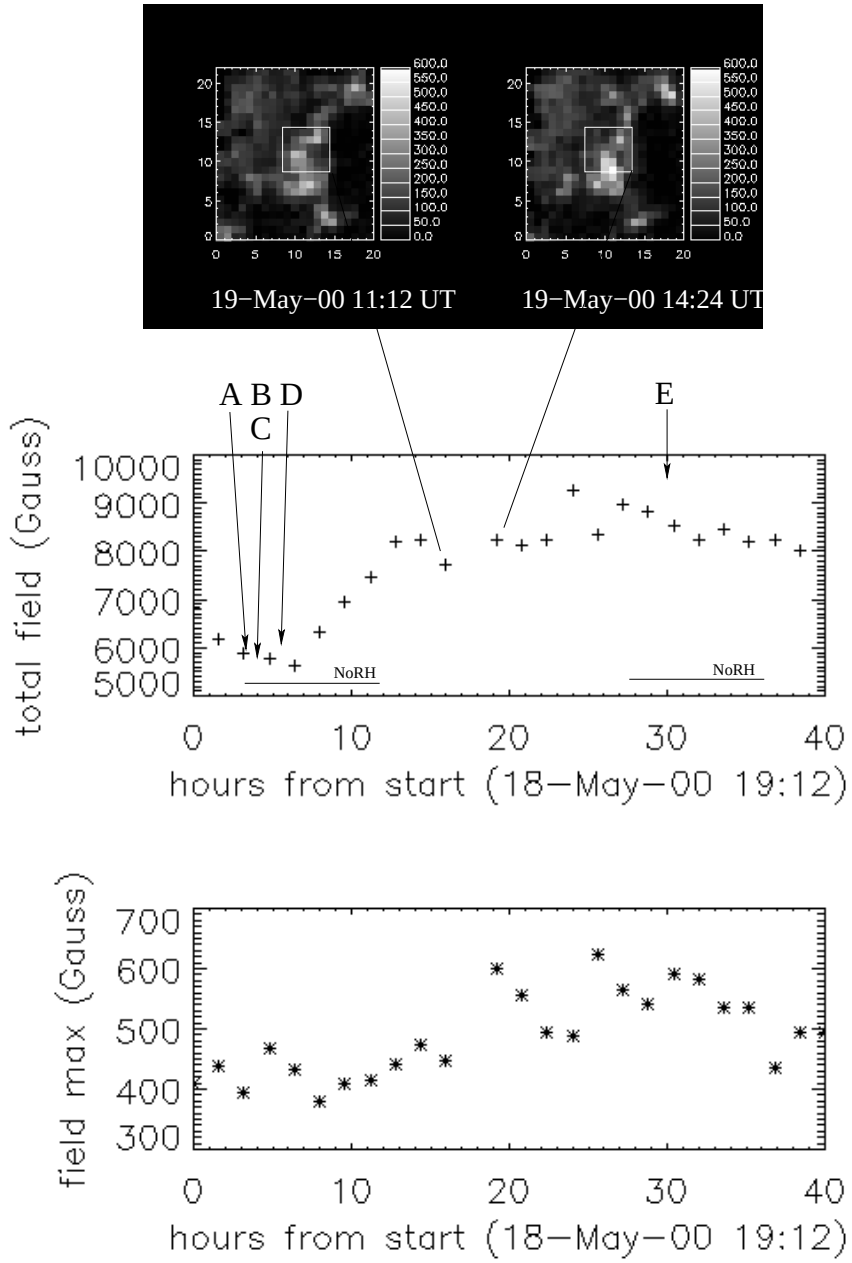

Figure 11. Evaluation of the field strength changes caused by the moving magnetic elements: *SOHO* MDI magnetograms at 11:12 and 14:24 UT on May 19, 2000, with the boxes that show the 6×6 pixel area from which the total and maximum magnetic field strength values (G) were calculated between May 18, 2000 19:12 UT and May 20, 2000 11:12 UT. The box contains mainly positive polarity flux. The MDI noise level is around 20 G. Arrows and letters indicate the times of flares A–E. NoRH observing times are also marked. Note how the bright positive polarity flux elements enter the box in the second image.

radio type III bursts observed around the time of the burst maximum indicate that some of the electrons had gained access to open field lines. In the absence of spatial information for the type III radio emission we cannot confirm the type III burst source location. Periodic fluctuations were observed both in the radio emission and in the hard X-ray count rates. No shift was observed in the radio emission location, but some of the HXT count rate peaks were located at different positions. No time delays were observed between the radio and hard X-ray flux peaks.

The emission mechanism for the hard X-ray source is most likely thick-target bremmstrahlung, as the accelerated electrons hit the dense loop footpoint area. The radio spectra for the radio emission source is typical for a gyrosynchrotron source with mildly energetic electrons: the observed spectral turn-over frequency was around 12 GHz, spectral index $\sim$-1.0, and the burst duration was about 1 minute. Strong radio emission coming from one footpoint area with a much higher magnetic field strength than in the other footpoint is acceptable, as gyrosynchrotron emission is sensitive mainly to the magnetic field strength and the viewing angle.

The proposed scenario in this case would be that electrons were accelerated somewhere along the two loops and the ones streaming towards the radio-emitting footpoint were mirrored back in the strong magnetic field emitting gyrosynchrotron radiation on the way (but no hard X-rays), but at the other footpoint with weaker magnetic field most of the electron population was lost as they hit the dense atmosphere (and emitted in hard X-rays but not in radio). Strong mirroring requires strong magnetic fields and the footpoint area near the sunspot (-1300 – -900 G) would be sufficient. In addition, if we assume the energy range of the accelerated electrons to be the same in both loops the 70 sfu radio emission at 17 GHz near 900 G magnetic field would bring only 1.5 sfu flux density near a 250 G field (emissivity is proportional to B^3). Exact calculations are difficult as we do not know the magnetic field strengths at coronal altitudes where radio emission most likely originates.

The above-mentioned findings support a model in which the two long-lived loops interact above the positive polarity field. A schematic drawing of a possible loop-loop interaction that could explain the observations is presented in Figure 12. The drawing presents only some of the loops and one should bear in mind that in reality these are complicated loop systems that contain bundles of loops. However, the EIT and SXT images show how almost all the field lines connect from the negative polarity sunspot region to some part of the positive polarity plage region, although in many of the images it is impossible to say which loop overlies which.

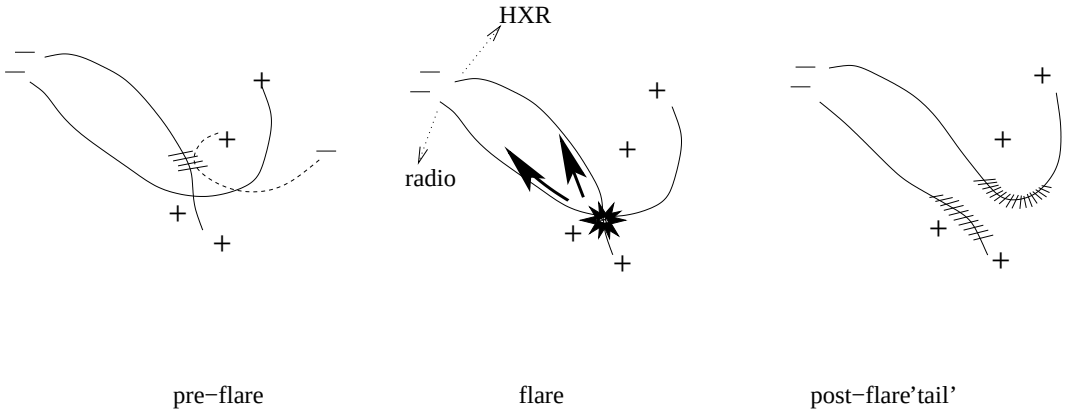

Figure 12. Schematic drawing of a possible loop-loop interaction that would result in a similar flare loop configuration that was observed on May 20, 2000 at 01:06 UT. Plus and minus signs indicate the magnetic field polarity and the hatched areas represent bright loop tops. Earlier interaction with the small loop (dotted line) is thought to be responsible for the upper loop brightening that leads to interaction with the lower loop.

The most probable acceleration site for the electrons observed during the impulsive part of the flare would therefore be the loop intersection in the plage region which was already bright in soft X-rays before the impulsive flare started. This early SXT brightening is loop top emission in the 'upper' loop that could be due to earlier interaction with the smaller vertical loop (during *Yohkoh* night time). Traces of this small loop (shown as dotted line in Figure 12) were seen in the SXT images before the flare (e.g., in Figure 3), but it seems evident this loop did not take part in the impulsive flare phase as it's footpoints did not show any brightenings. The cause for this 'first interaction' between the small loop and the long-living upper loop could be the spatial shifts in the positive polarity flux elements. Some evidence for this was shown in Figure 11, as the magnetic field strength inside the box, around the small loop footpoint area, increased by $\sim$ 1000 G before flare E.

The SXT lightcurves for the different footpoint regions and the long-living loops revealed that they all brightened during the flare. The simultaneous emission and fluctuations in radio and X-rays – at two different loop footpoints – further support the idea of a single acceleration site that supplies high energy electrons to both of the two connecting loops. The later 'thermal tail' emission comes mainly from the upper loop that had changed positive polarity footpoints with the lower loop in reconnection, and is then filling up in hot and dense plasma (as shown in Figure 6f).

The observed fluctuations in the radio emission could be explained either by fluctuations in the number of particles in the acceleration process or by transverse oscillations of the flare loop at the Alfvén speed, v_A, (see example in, e.g., Pohjolainen et al., 1997). Number variations in the acceleration process would mean continuous acceleration, and Alfvénic oscillations could be due to upward motions of hot evaporated plasma. The similar time profiles of the radio and hard X-ray emission, with no evident time delays, would suggest a continuous acceleration process with electrons streaming down both of the loops. This would mean that similar particle populations would have to be injected simultaneously to the two loops (i.e., these loops would have to interact). At the other end of the loops in the plage region the lack of impulsive emission in radio and hard X-rays could simply be masked by the observed thermal emission coming from that region.

Hence, was this repeated flaring created by stored magnetic energy that was released by continual shearing motions or by repeatedly emerging flux? In fact, the homology in this case does not imply that only one mechanism is possible – the repeated flaring was located at the footpoints of the two long-living loops situated at the outskirts of the strong sunspot region and in principle both mechanisms are possible at the other end of the loops as long as the mechanism does not destroy these loops. In principle, an emerging loop (bipolar region) near the plage area could directly cause the flaring as in the scenario presented by Hanaoka (1997) and Heyvaerts, Priest, and Rust (1977), but this type of loop-loop interaction would then have to involve both of the pre-existing loops. In other words, because of the single acceleration process along both of the loops the emerging loop would have to interact with both of them simultaneously, which would require special conditions that would also be difficult to repeat. No real evidence of emerging flux near the loop ends was found. Instead, spatial shifts were observed in the positive polarity flux elements and a small loop was observed at earlier times at the same location – a possible cause for the pre-flare brightening of the upper loop. Flare models based on shear-driven quadrupolar reconnection have been reviewed by Aschwanden (1999) and this mechanism could be applied for the pre-flare brightening of the upper loop: the interacting small loop had a positive polarity footpoint in the region that was shown to undergo spatial changes. Magnetic reconnection triggered by thermal instability (e.g., by the existence of hot and cool loops after a flare) has recently been suggested by Kliem et al. (2002), and in this case both a hot (the brightened upper loop) and a cooler (lower extended loop) SXT loop did exist.

As this complex magnetic region contained at least two long-living loops and there was also evidence of footpoint motions we suggest that

the repeated flaring was due to loop-loop interactions of pre-existing loops. The similar characteristics of the flares in this series suggest that the mechanism – and the loop footpoints – were the same in all cases.

Acknowledgements

The author is grateful to the Japan Society for the Promotion of Science for supporting a visit to the Nobeyama Radio Observatory, NAOJ. The people at Nobeyama and ISAS are thanked for assistance in data analysis. J.I. Khan and K. Shibasaki are thanked for discussions and comments on the manuscript, and the anonymous referee for perceptive comments on how to improve the paper. Nobeyama Radioheliograph and Polarimeters are operated by Nobeyama Radio Observatory/NAOJ. The Hiraiso Radio Spectrograph is operated by the Communications Research Laboratory, Japan. *Yohkoh* is a mission of the Institute of Space and Astronautical Sciences, Japan, with participation from the US and U.K. *SOHO* is a project of international cooperation between ESA and NASA. Hα images are obtained from the Space Environment Center Database, Boulder, National Oceanic and Atmospheric Administration. The BATSE Solar Flare Database is maintained at the Solar Data Analysis Center at Goddard Space Flight Center.

References

Aschwanden, M.: 1999, in T.S. Bastian, N. Gopalswamy and K. Shibasaki (eds): Proc. of the Nobeyama Symposium, NRO Report No. 479., 307
Choe, G.S. and Cheng, C.Z.: 2000, *Astrophys. J.* **541**, 449.
Cliver, E. and Wefer, F.L.: 1981, *Solar Phys.* **71**, 39.
Delaboudinière, J.-P., et al.: 1995, *Solar Phys.* **162**, 291.
Fishman, G. J., Meegan, C. A., Wilson, R. B., Brock, M. N., Horack, J. M. et al.: 1994, *Astrophys. J. Suppl. Ser.* **92**, 229.
Gaizauskas, V.: 1986,*Solar Phys.* **105**, 67.
Hanaoka, Y.: 1997,*Solar Phys.* **173**, 319.
Heyvaerts, J., Priest, E.R., and Rust, D.M.: 1977, *Astrophys. J.* **216**, 123.
Howard, R.F., Harvey, J.W., Forgach, S.: 1990, *Solar Phys.* **130**, 295.
Howard, R., and Svestka, Z.: 1981 *Solar Phys.* **71**, 49.
Kliem, B., Dammasch, I.E., Curdt, W., and Wilhelm, K.: 2002, *Astrophys. J.* **568**, 568, L61
Kosugi, T., et al.: 1991, *Solar Phys.* **136**, 17.
Machado, M.E.: 1985, *Solar Phys.* **99**, 159.
Martres, M.J.: 1989, *Solar Phys.* **119**, 357.
Nakajima, H., et al.: 1985, PASJ **37**, 163.
Nakajima, H., et al.: 1994, *Proc. IEEE* **82**, 705.

Pohjolainen, S., Valtaoja, E., Urpo, S., and Aurass, H.: 1997, *Solar Phys.* **173**, 131.
Ranns, N.D.R., Harra, L.K., Matthews, S.A., and Culhane, J.L.: 2000, *Astron. Astrophys.* **360**, 1163.
Scherrer, P.H., et al.: 1995, *Solar Phys.* **162**, 129.
Sterling, A.C., and Moore, R.L.: 2001, *Astrophys. J.* **560**, 1045.
Tsuneta, S. et al.: 1991, *Solar Phys.* **136**, 37.
Zhang, J., and Wang, J.: 2002, *Astrophys. J.* **566**, L117.
Zirin H.: 1983, *Astrophys. J.* **274**, 900.